LAWRENCE
LIVERMORE
NATIONAL
LABORATORY

LLNL-JRNL-669534

Mesoscale particle-based model of electrophoresis

B. Giera, L. Zepeda-Ruiz, A. Pascall, T. Weisgraber, J. Kuntz, C. Spadaccini

April 13, 2015

Journal of the Electrochemical Society

Disclaimer

Mesoscale particle-based model of electrophoresis

Brian Giera,[*1] Luis A. Zepeda-Ruiz,[*2] Andrew J. Pascall, Joshua D. Kuntz, Christopher M. Spadaccini, and Todd H. Weisgraber

Center for Micro- and Nano-Technology, Lawrence Livemore National Laboratory, Livermore, California 94551, USA

Abstract

We develop and evaluate a semi-empirical particle-based model of electrophoresis using extensive mesoscale simulations. We parameterize the model using *only* measurable quantities from a broad set of colloidal suspensions with properties that span the experimentally relevant regime. With sufficient sampling, simulated diffusivities and electrophoretic velocities match predictions of the ubiquitous Stokes-Einstein and Henry equations, respectively. This agreement holds for non-polar and aqueous solvents or ionic liquid colloidal suspensions under a wide range of applied electric fields.

Cite as:

Brian Giera, Luis A. Zepeda-Ruiz, Andrew J. Pascall, Joshua D. Kuntz, Christopher M. Spadaccini, and Todd H. Weisgraber. "Mesoscale particle-based model of electrophoresis." *J. Electrochem. Soc.* 2015 Vol.162, **issue 11**, D3030-D3035.

doi: 10.1149/2.0161511jes

[*]To whom correspondence should be addressed

[1]giera1@llnl.gov

[2]zepedaruiz1@llnl.gov

1 Introduction

Electrophoresis describes the movement of charged particles dispersed in a fluid due to applied electric fields. Colloids comprised of ceramics,[1] carbon nanotubes,[2] nanometals,[3] polymers,[4] phosphors,[5] and biological materials[6] undergo electrophoretic motion in response to an applied electric field that acts upon the charged interface between the particle and surrounding suspension. Some examples of the suspension media are aqueous[7] and non-polar[8] solvents, liquid crystals,[9] or ionic liquids.[10] In addition to the applied field strength, the electrophoretic velocity depends on the ionic strength, permittivity, and viscosity of the suspension as well as the potential difference between the surface of the colloid and suspension (termed the zeta-potential). Electrophoresis is central to electrophoretic deposition (EPD) in which field-driven particles accumulate at electrodes or liquid-liquid interfaces[11] to form layers that are stabilized by short-ranged van der Waals interactions.[12]

Recently, EPD using photoconductive electrodes was demonstrated to be an effective additive manufacturing (AM) technique to produce sophisticated patterns of multimaterial 3D composites.[13] Another EPD AM strategy builds objects from lines of colloids that are selectively deposited using coaxial cable electrodes.[14,15] Furthermore, precise control of individual particle(s) placement is possible with EPD onto patterned electrodes.[16] Enhanced control of the shape, composition, and performance of functional materials fabricated via EPD AM can benefit from computationally feasible models that predict transient colloidal depositions lasting seconds to minutes. A suitable model of EPD must also capture the diffusivity and electrophoretic mobility, which collectively characterize the stability and mass transport of colloidal suspensions.[17] The electric field strength, suspension properties, zeta-potential, and colloid radius all influence electrophoretic and Brownian motion. In turn, the relative magnitude of convective and diffusive colloidal motion, as defined by the dimensionless Péclet number (Pe), influences the packing quality of colloidal deposits. For instance, colloidal deposits exhibit crystalline packing at low Péclet (where diffusive motion dominates) and amorphous deposits form at large Péclet (where convective motion dominates).[18]

The majority of colloidal suspension models give continuum level descriptions of electrophoresis and EPD.[19] Models of EPD kinetics predict mass deposition rates that depend (at least) on the electrophoretic velocity, electrode surface area, and fraction of colloids that stick to the deposit.[1,20,21] Film thickness models suggest the relative values of the particle and suspension permittivities dictate the deposit uniformity.[22] Finite and discrete element[23,24] models elucidate how deposit morphology depends on electrode edge effects and particle area fraction, electrolyte pH, and current density, respectively. Two commonly-used analytical models of bulk Brownian and electrophoretic motion include the Stokes-Einstein[25] and Henry equations,[26] respectively. The Stokes-Einstein equation gives the diffusivity of a dilute dispersion of spherical particles. The Henry equation predicts the electrophoretic velocity of colloids with any shape[27] to depend linearly on the field, solvent permittivity, zeta-potential, and inversely to viscosity. It is used widely to infer the zeta-potential from electrophoretic velocity measurements obtained via light-scattering techniques.[28] Despite their widespread use, continuum EPD models inherently neglect particle-based descriptions of colloidal suspensions. These inter-colloidal interactions are necessary to understand the underlying physics that govern the formation and microstructure of the deposit.

There are a variety of modeling techniques that treat colloidal particles explicitly with pairwise potentials. Methods are subdivided according to whether the coarse-grained solvent is treated explicitly (by simulating additional solvent particles) or implicitly (by incorporating additional terms to the pairwise colloid potentials). Dissipative Particle Dynamics (DPD) model solvent interactions explicitly with particles that represent spherical blobs of fluid that interact through momentum-preserving collisions.[29] Although a mesoscale DPD electrophoresis model qualitatively reproduced aspects of the Henry equation in a limited regime,[30] the results pertain to a generic DPD system and were not easily relatable to a specific experimental system. Stochastic Particle Dynamics (SPD) is a similar, albeit more efficient, method than DPD, which easily can be parameterized to recover desired suspension viscosity values.[31] However, as with coarse-grained explicit solvent models, it is problematic

to map measurable properties entirely from a specific colloidal suspension to DPD or SPD models and vice versa.[32] Recently, Fast Lubrication Dynamics (FLD) implicit solvent models exhibited superior accuracy and computational expense than explicit solvent approaches.[33] As an added benefit, the suspension properties are input directly into the FLD model. Using inertial FLD, mesoscale molecular dynamics simulations of an aqueous suspension of polystyrene colloids reproduced experimentally measured diffusivities at several volume fractions.[32,33] Although only a limited range of suspension parameters were interrogated to validate simulated diffusivities, the results prove it is possible to model colloids undergoing purely diffusive motion up to hundreds of seconds. In spite of the available models in the literature, a model of colloidal suspensions under applied fields has not been presented that suitably captures electrophoretic phenomena.

In this article, we augment implicit solvent mesoscale approaches to develop a semi-empirical particle-based model that accurately captures the electrophoretic motion of colloids over a comprehensive range of experimentally relevant conditions. We extensively parameterize the model using *only* measurable quantities in order to map out the regime where this approach adequately describes the dynamics of homogenous monodisperse colloidal suspensions. We show that, with sufficient sampling, simulated diffusivities and electrophoretic velocities match predictions from the Stokes-Einstein and Henry equations across an enormous range of Péclet numbers: $0 \leq \mathrm{Pe} < 10^8$. This validation is a necessary step towards developing an accurate model of EPD AM.

2 Model Details

The mesoscale model for electrophoresis that we use includes internal and external forces, given by

$$\mathbf{F}_{\mathrm{total}} = \mathbf{F}_{\mathrm{Hydro}} + \mathbf{F}_{\mathrm{Brown}} + \mathbf{F}_{\mathrm{DLVO}} + \mathbf{F}_{\mathrm{field}}. \tag{1}$$

The first three terms represent the internal forces that account for implicit solvent-colloid ($\mathbf{F}_{\text{Hydro}}, \mathbf{F}_{\text{Brown}}$) and colloid-colloid ($\mathbf{F}_{\text{DLVO}}$) interactions. The last term ($\mathbf{F}_{\text{field}}$) is the external driving force due to a uniformly applied electric field. All these components are implemented in the Large-scale Atomic/Molecular Massively Parallel Simulator (LAMMPS).[34]

The solvent model[35,36] implicitly incorporates dissipative lubrication forces $\mathbf{F}_{\text{Hydro}}(\mathbf{r};\eta)$ and Brownian contributions $\mathbf{F}_{\text{Brown}}(\mathbf{r};T)$ between nearby colloids at positions $\mathbf{r}$ in a continuum suspension with uniform viscosity η and temperature T. Steric, van der Waals, and electrostatic inter-colloidal forces $\mathbf{F}_{\text{DLVO}}(\mathbf{r};a,A^{\text{col}},\lambda_{\text{D}},A^{\text{Yuk}})$ are treated within the Derjaguin-Landau-Verwey-Overbeek[37,38] (DLVO) framework. The former terms are modeled by a widely-used pairwise potential with characteristic size a and Hamaker constant A^{col}.[39] The latter term describes electrostatic repulsion between electric double layers formed by ions in the fluid that screen the surface charge of colloids over the characteristic Debye length λ_{D}. This also is modeled in a pairwise fashion with a variant of the Yukawa potential[40] with interaction constant A^{Yuk} that is set by the zeta-potential ζ, relative permittivity ϵ, ion valence q, and temperature.[41] In their present form, the above three pairwise interactions model colloids without surface conductance and double layer distortion. The external force that causes electrophoresis $\mathbf{F}_{\text{field}}(\mathbf{E};q^{\text{col}})$ depends on the applied electric field $\mathbf{E}$ acting on a colloid with effective charge q^{col}

$$\mathbf{F}_{\text{field}} = q^{\text{col}}\mathbf{E}. \tag{2}$$

For simplicity, here we simulate bulk electrophoretic motion along a single direction with uniform electric field with strength E_z. In this work, we apply electric fields beyond the dielectric strength of fluids ($\sim 10^8$ V/m) in order to ensure we have validated the model for all experimentally realizable fields. For clarity, Table 1 summarizes the complete list of measurable properties that fully specifies this colloidal suspension model.

It is crucial to assign the correct value for the effective charge of colloids in Equation 2. This is determined from the total force acting on a colloid experiencing hydrodynamic drag

Table 1: Summary of parameters that fully specifies a mesoscale molecular dynamics simulation of a colloidal suspension. For ease of discussion, we express all simulations relative to a model reference system that is configured using only measurable properties from a colloidal suspension of polystyrene particles in 10% ethanol. We validate the model across the simulated range of model parameters (rightmost column) that comprehensively spans experimentally relevant colloidal suspensions undergoing electrophoresis.

Parameter	**Symbol**	**Reference Value**	**Simulated Range**
Colloid density	ρ^{col}	1050×10^3 g/m^3	$\rho^{\text{col}} = \rho^{\text{col}}_{\text{ref}}$
Hamaker constant	A^{col}	10^{-20} J	$A^{\text{col}} = A^{\text{col}}_{\text{ref}}$
Electrolyte valence	q	1	$q = q_{\text{ref}}$
Zeta potential	ζ	-0.05 V	$-0.5 \leq \zeta/\zeta_{\text{ref}} \leq 1$
Relative permittivity	ϵ	40	$0.05 \leq \epsilon/\epsilon_{\text{ref}} \leq 2$
Temperature	T	300 K	$2/3 \leq T/T_{\text{ref}} \leq 1$
Dynamic viscosity	η	10^{-3} Pa $\cdot$ s	$0.1 \leq \eta/\eta_{\text{ref}} \leq 10$
Colloid radius	a	100×10^{-9} m	$0.01 \leq a/a_{\text{ref}} \leq 10$
Debye length	λ_{D}	50×10^{-9} m	$a/\lambda_{\text{D}} = 2$
Electric field strength	E_{z}		$0 - 10^{12}$ V/m

in an electric field moving with steady-state velocity $\mathbf{U}$[26,42]

$$-6\pi\eta a\mathbf{U} + 6\pi\zeta a\epsilon_0\epsilon\left(1 + 5a^5\int_\infty^a \frac{\phi(\hat{r})/\zeta}{\hat{r}^6}\mathrm{d}\hat{r} - 2a^3\int_\infty^a \frac{\phi(\hat{r})/\zeta}{\hat{r}^4}\mathrm{d}\hat{r}\right)\mathbf{E} = 0. \tag{3}$$

In Equation 3, the potential distribution of ions, $\phi(r)$, is taken to be the well known linearized Debye-Hückel approximation that DLVO theory assumes. From Eqns. 2 and 3, the effective charge of the colloid is given by

$$q^{\text{col}} = \frac{\pi\zeta a\epsilon_0\epsilon}{24\lambda_{\text{D}}^6}\left(a^5\lambda_{\text{D}} - a^4\lambda_{\text{D}}^2 - 10a^3\lambda_{\text{D}}^3 + 6a^2\lambda_{\text{D}}^4 + 96\lambda_{\text{D}}^6 + a^4\left(12\lambda_{\text{D}}^2 - a^2\right)e^{a/\lambda_{\text{D}}}\int_1^\infty \frac{e^{-a\hat{g}/\lambda_{\text{D}}}}{\hat{g}}\mathrm{d}\hat{g}\right), \tag{4}$$

where ϵ_0 is the permittivity of free space. Another intuitive, albeit incorrect, approach is to assign q^{col} solely from the Debye-Hückel expression that relates the effective colloid charge to the zeta-potential

$$q^{\text{col}}_{\text{DH}} = 4\pi a^2\epsilon_0\epsilon\zeta\left(\frac{1}{a} + \frac{1}{\lambda_{\text{D}}}\right). \tag{5}$$

For the case of infinitely dilute electrolytes, $\lambda_D \to \infty$ and $\{q^{col}, q^{col}_{DH}\} \to 4\pi a \epsilon_0 \epsilon \zeta$. Using the reference values in Table 1, Eq. 4 gives $q^{col} = -2.37 \times 10^{-17}$ C while Eq. 5 gives $q^{col}_{DH} = -6.28 \times 10^{-17}$ C. Although these two values are the same magnitude, using q^{col}_{DH} results in computed electrophoretic velocities that are $6.28/2.37 \approx 2.65$ times larger than Henry equation predictions. Only when we use the correct expression for q^{col} from Eq. 4, do our model results collapse onto the Henry equation over the entire simulated range of applied fields in Table 1, as we detail in Section 3.

In order to efficiently simulate bulk electrophoresis, we use the largest allowable time step for a given suspension viscosity and colloid size, e.g. the most viscous suspension $\eta = 10$ mPa $\cdot$ s with the smallest colloid diameter $a = 1$ nm simulated permits $\delta t = 10^{-5}$ ns while $\delta t \leq 10^3$ ns is possible in the opposite limit. Thus, with reasonable computational resources, it is possible to reach simulation times spanning several minutes. For all simulations performed here, we set the number of particles $N^{col} = 1000$ within a total volume $V = (200a)^3$ in order to fix the volume fraction of colloids $\approx 7 \times 10^{-5}$. This dilute regime, which characterizes systems with long mean-free paths, is computationally inexpensive to simulate because pairwise interactions ($\mathbf{F}_{Hydro}$, $\mathbf{F}_{Brown}$, and $\mathbf{F}_{DLVO}$ in Eq. 1) only are calculated for closely separated colloids. In what follows, we evaluate simulations of dilute dispersions of colloids that cover the comprehensive range of material properties and experimental conditions given in Table 1.

3 Results and Discussion

Here, we systematically validate the principle components of the model by comparing simulated diffusivities and velocity distributions to the Stokes-Einstein and Henry equations under a variety of conditions. Our evaluation begins by assessing how well the model captures pure Brownian motion of colloids in the dilute regime where the Stokes-Einstein equation is

valid[25]

$$\mathcal{D}_{\mathrm{SE}} = \frac{k_{\mathrm{B}}T}{6\pi\eta a}\,, \tag{6}$$

with Boltzmann's constant k_{B}. We benchmark the model against equation 6 with the standard Einstein relation[25]

$$\mathcal{D}_{\mathrm{sim}} = \frac{1}{6}\lim_{t\to\infty}\frac{d}{dt}\langle|\mathbf{r}(t)-\mathbf{r}_0|^2\rangle \tag{7}$$

to compute the diffusivity from the slope of the mean squared displacement at long times. Equation 7 is computed by subtracting particle coordinates taken directly after 2×10^6 time steps of equilibration, $\mathbf{r}_0$, from time-dependent particle coordinates, $\mathbf{r}(t)$, which are collected for at least 3×10^9 time steps. Figure 1 shows quantitative agreement between $\mathcal{D}_{\mathrm{sim}}$ and $\mathcal{D}_{\mathrm{SE}}$ over a range of simulations of model liquid colloidal suspensions. The simulated diffusivities fall within 5.6% of $\mathcal{D}_{\mathrm{SE}}$ and the error, as defined by the standard deviation of 10 independent simulations, is within 10% of $\bar{\mathcal{D}}_{\mathrm{sim}}$. The results in Figure 1 are complementary to recent work by Bolintineanu, et. al.[33] in which they validate the same implicit solvent model with a single suspension viscosity simulated over a range of colloid volume fractions.

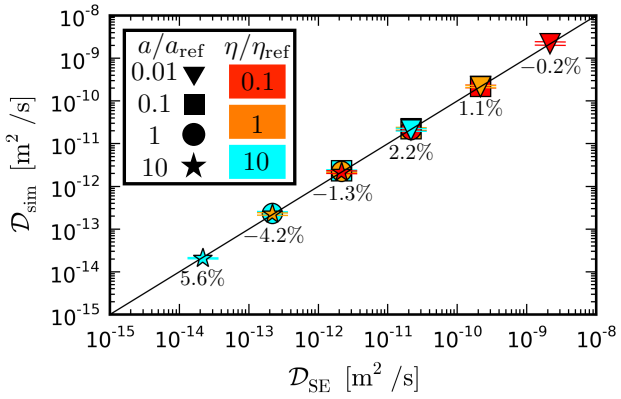

Figure 1: Simulated diffusivities, $\mathcal{D}_{\mathrm{sim}}$, are compared against the Stokes-Einstein results, $\mathcal{D}_{\mathrm{SE}}$, for a dozen colloidal suspensions (legend). Markers are plotted at the average value of 10 independent simulations with error bars computed from the standard deviation. The diffusion constants quantitatively agree across six orders of magnitude of computed values as indicated by the averaged deviations $1-\bar{\mathcal{D}}_{\mathrm{sim}}/\mathcal{D}_{\mathrm{SE}} \leq \pm 5.6\%$.

Having validated the implicit solvent model to reproduce Stokes-Einstein diffusivities

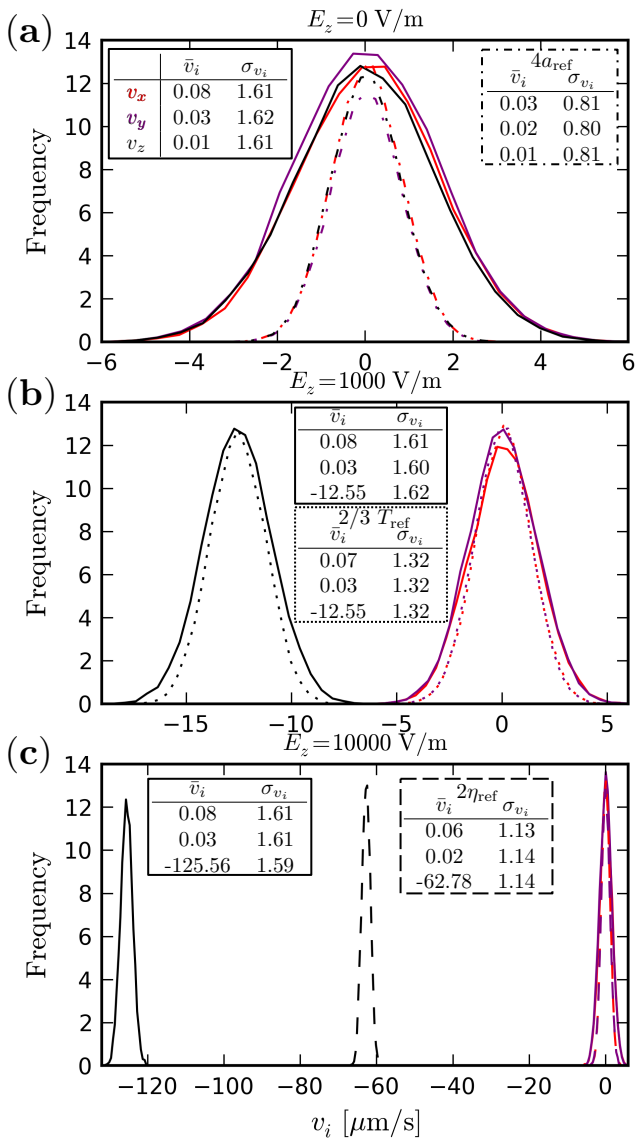

Figure 2: Velocity component distributions (v_x, v_y, and v_z in red, purple, and black, respectively, with means and standard deviations in legends) that are sampled from 20 two-second simulation trajectories of the reference system (solid lines, a-c) under three electric fields (titles) and non-reference suspensions with larger colloids $a = 400$ nm (dash-dotted lines, a), lower system temperature $T = 200$ K (dotted lines, b), and higher viscosity $\eta = 2$ mPa $\cdot$ s (dashed, c). (a-c) The standard deviation is invariant to the applied field and exhibits the scaling $\sigma_{v_i} \sim \sqrt{T/\eta a}$. (a) Without an applied field, the distributions for a given system are indistinguishable with mean values $\bar{v}_i \approx 0$. (b-c) With fields applied in the $+z$-direction, negatively charged colloids move against the applied electric field with a mean electrophoretic velocity that scales like $\bar{v}_z \sim E_z/\eta$. (a-c) Irrespective of the field, $\bar{v}_x \approx \bar{v}_y \approx 0$.

across a wide range of colloid sizes and suspension viscosities, we now take a detailed look at the interplay between the colloidal suspension pairwise potentials and the uniformly applied field. Specifically, we examine how the colloidal velocity distributions depend on the applied field strength, colloid size, and suspension temperature and viscosity with which we initialize the model. We determine the steady-state velocity of each colloid i from the slope of particle displacement

$$\mathbf{v}^i = \lim_{t\to\infty} \frac{d}{dt}\left(\mathbf{r}^i(t) - \mathbf{r}_0^i\right) \tag{8}$$

from simulation trajectories that span 2 seconds. Figure 2 shows velocity component histograms $\{v_x, v_y, v_z\}$ that are sampled from 20 independent simulations. Figure 2(a-c) includes velocity distributions for the reference system under three experimentally accessible fields applied only in the z-direction: $E_z = \{0, 10^3, 10^4\}$ V/m. At each field, we also display distributions from suspensions simulated with larger colloids Figure 2(a), lower system temperature Figure 2(b), and higher viscosity Figure 2(c) than the reference system. The standard deviation of each velocity component distribution, σ_{v_i} is due to Brownian fluctuations imparted by the implicit solvent. Comparing the reference system to the other simulated suspensions reveals the magnitude of these fluctuations to scale by $\sigma_{v_i} \sim \sqrt{T/\eta a}$. The electrophoretic, v_z, and purely Brownian velocity components, v_x and v_y, exhibit normal distributions with the same width, i.e. within a given system $\sigma_{v_x} \approx \sigma_{v_y} \approx \sigma_{v_z}$. Since we model an isothermal system, the external driving force imparted by the applied field does not affect Brownian motion.

In the absence of a field Figure 2(a), the velocity distributions are equivalent $\bar{v}_i \approx 0$. The mean of the velocity component parallel to the applied field $\bar{v}_z$ is directly proportional to the applied field while $\bar{v}_x \approx \bar{v}_y \approx 0$ rigorously for any E_z. As expected from the Henry equation, electrophoresis is invariant to the temperature of the colloidal suspension Figure 2(b). In Figure 2(c), the electrophoretic velocity scales like the Henry equation, e.g. $\bar{v}_z$ is halved as η is doubled from the reference value. With a limited set of simulations, Figure 2 illustrates, in part, the relative impact the applied field strength and colloidal suspension properties have

on electrophoretic and diffusive motion. Crucially, the thermostatting algorithm and hydrodynamics interactions do not interfere with the flow characteristics of convecting colloids.

We now compare values for the electrophoretic velocity computed from the model directly to the Henry equation[26]

$$v_{\mathrm{H}} = \frac{2}{3}\frac{E_z \zeta \epsilon \epsilon_0}{\eta} f\left(\frac{a}{\lambda_{\mathrm{D}}}\right). \tag{9}$$

The Henry function, $f\left(a/\lambda_{\mathrm{D}}\right)$, accounts for suspensions with arbitrarily thick double-layers and monotonically varies from $f(a/\lambda_{\mathrm{D}} \to 0) \to 1$ in the thin double-layer limit to $f(a/\lambda_{\mathrm{D}} \to \infty) \to 3/2$ in the reverse limit. Importantly, equation 9 and our model assume uniformly thick double-layers and negligible surface conductance and thus are strictly valid for infinitesimal values of the dimensionless Dukhin number (ratio of surface to bulk conductance $\to 0$).[43] In the large Dukhin limit where surface conductance matters, the nonlinearities in the electrophoretic velocity that arise[44–46] are beyond the scope of this work. Since the Henry equation predicts electrophoresis to be invariant of volume fraction,[47] we proceed to validate the model in the dilute regime with computationally efficient simulations. We simulate an array of 54 distinct model systems with $a/\lambda_{\mathrm{D}} = 2$ by systematically varying across 4 orders of magnitude in a, 3 orders of magnitude in η, 2 orders of magnitude in ϵ, and positive and negative values of ζ. For each system, we use equation 8 to compute average electrophoretic velocities from a series of simulations in which we increase the applied field strength. Figure 3 shows a subset of 28 model systems with simulated electrophoretic velocities that match the Henry equation. We found comparisons between model systems with extremely thick $a/\lambda_{\mathrm{D}} = 0.02$ and thin $a/\lambda_{\mathrm{D}} = 200$ double layers to be equivalent to Figure 3. For all simulations, the average deviation between the model and Henry equation is $\overline{1 - v_{\mathrm{H}}/\bar{v}_{\mathrm{z}}} < \pm 0.48\%$ across 11 orders of magnitude of computed $\bar{v}_z$. However, the dimensional plots displayed in Figure 3 make it difficult to discern potential deviations of $\bar{v}_z$ from v_{H}.

The model validation is not restricted to colloidal suspensions with only the exact measurable properties that we use here. By non-dimensionalizing the system with a Péclet number

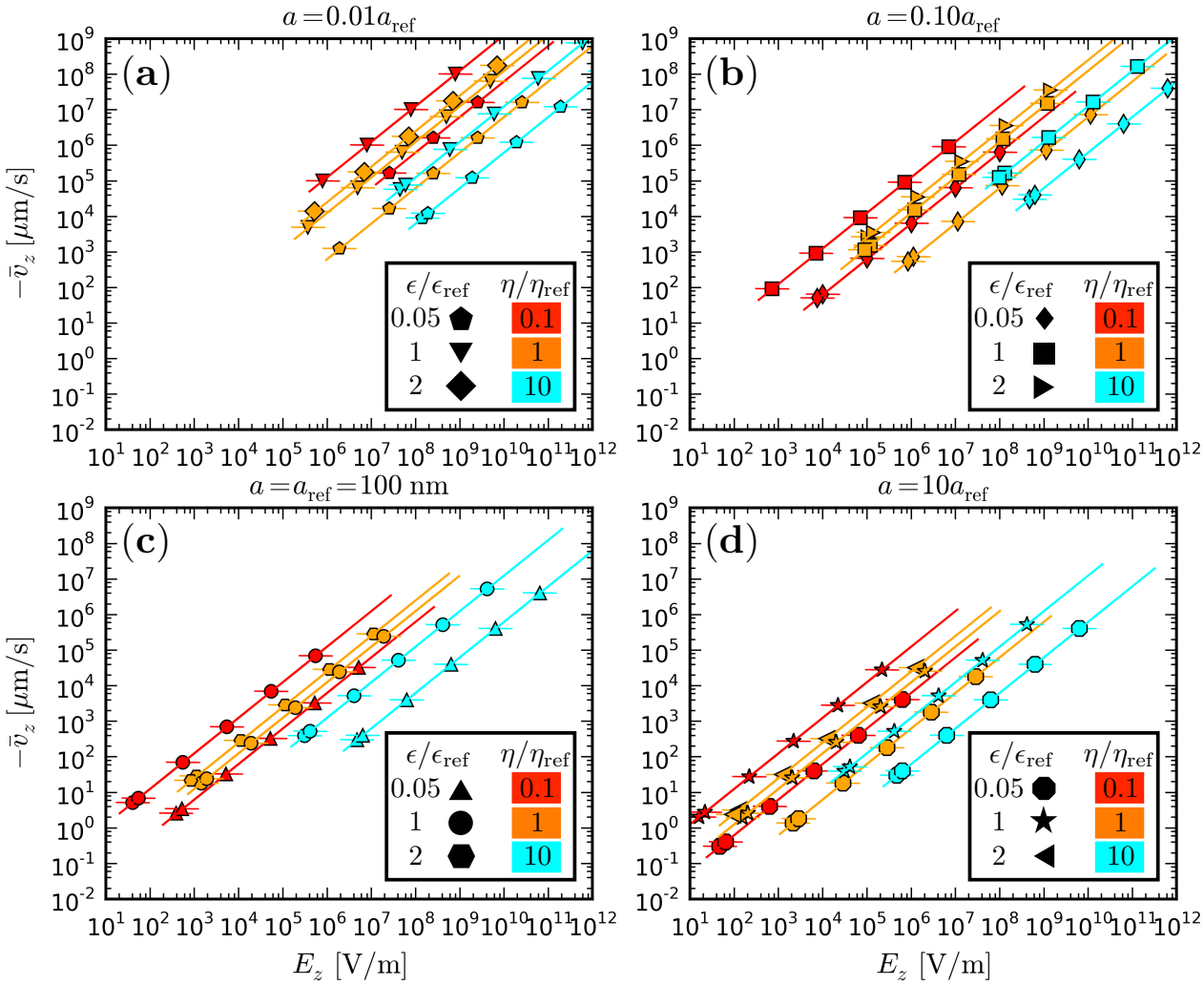

Figure 3: Electrophoretic velocities from simulation quantitatively agree with the Henry equation 9 (lines) for colloids with $\zeta_{\mathrm{ref}} = -0.05$ and radii $1 - 10^3$ nm (titles, a-d) in suspensions (legend) with a broad range of permittivities $\epsilon = \{2, 40, 80\}$ and viscosities $\eta = \{0.1, 1, 10\}$ mPa $\cdot$ s that characterizes non-polar solvents, aqueous electrolytes, and ionic liquids. Markers are plotted at the average value of 5 independent simulations with error bars computed from the standard deviation.

(ratio of convective to diffusive motion),

$$\mathrm{Pe} = \frac{|v_\mathrm{H}|}{\mathcal{D}_\mathrm{SE}} a = \frac{6\pi a^2 |E_z \zeta| \epsilon\epsilon_0}{k_\mathrm{B} T} f\left(\frac{a}{\lambda_\mathrm{D}}\right), \tag{10}$$

we show in Figure 4 that the model accurately captures electrophoretic motion of *any* experimentally relevant colloidal suspension with Péclet values $10^{-3} < \mathrm{Pe} < 10^{8}$. Figure 4 compares the Henry equation against simulated velocities from 54 model systems at 367 distinct Péclet values. The sample time for each simulation, τ, is adjusted so that the electrophoretic displacement of each colloid is approximately 10 diameters, i.e. $\tau \approx 20a/v_\mathrm{H}$. Thus, systems at low Péclet require longer computation times than at high Péclet. The standard deviation of 5 independent simulations defines the comparison error $\sigma_{v_\mathrm{H}/\bar{v}_z}$. The qualitative agreement is significantly better at higher Péclet, i.e. the error and maximum value of the deviation, $|1 - v_\mathrm{H}/\bar{v}_z|$, decrease at larger Pe. For instance, the maximum deviation for simulations is $\pm 5.6\%$ for $\mathrm{Pe} \leq 1$ and $\pm 0.71\%$ for $\mathrm{Pe} > 1$. We attribute deviations at lower Péclet to the difficulty of sampling the convective velocity component in regimes where Brownian motion dominates. For a single system at $\mathrm{Pe} = 0.03$ as shown in Figure 4(b), as the sampling window is increased from 15 to 150 minutes $\bar{v}_z$ approaches v_H and $\sigma_{v_\mathrm{H}/\bar{v}_z}$ drops by 70%. Additionally, the comparison error decreases with increasing Péclet as shown in Figure 4(c). This implies that, with longer sampling times at low Péclet, it is possible to minimize error between v_H and $\bar{v}_z$ to an arbitrary level.

4 Conclusions

We evaluate a semi-empirical model of electrophoresis by comparing extensive particle-based simulations against the Stokes-Einstein and Henry equations. The model accurately describes diffusive and electrophoretic motion of experimentally relevant colloidal suspensions. In the absence of an applied field, simulated diffusivities are within 5.6% of the Stokes-Einstein equation across six orders of magnitude. In the low Péclet regime ($\mathrm{Pe} \leq 1$) where

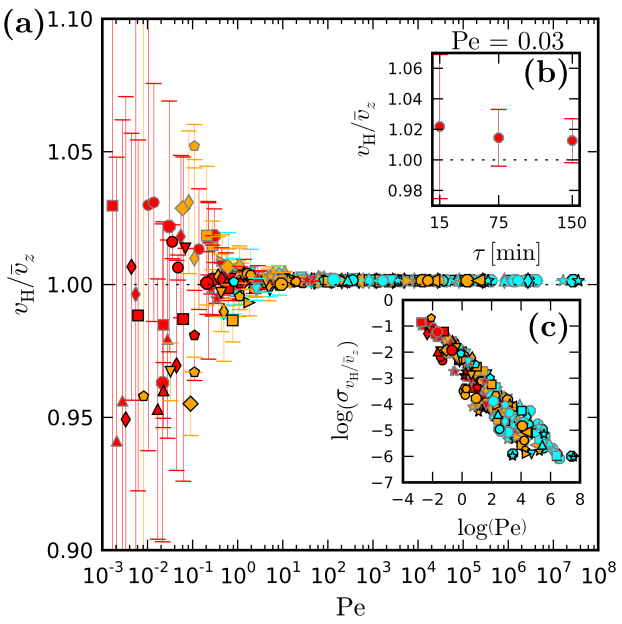

Figure 4: (a) The electrophoretic velocity from all simulations (Figure 3 legends with added grey-edged markers signifying $\zeta = 0.025$ V) and Henry equation agree within $\pm 5.6\%$ across all Péclet (equation 10) and converge $v_H/\bar{v}_z \leq 1 \pm 1\%$ for Pe ≥ 1. (b) Sampling longer trajectory times from a model system at Pe $= 0.03$ reduces the comparison error $\sigma_{v_H/\bar{v}_z}$ by 70% while $\bar{v}_z \to 0.99 v_H$ as $\tau \to 150$ minutes. (c) The comparison error decreases with increasing Pe and is negligible when electrophoretic motion dominates Brownian fluctuations, e.g. $\sigma_{v_H/\bar{v}_z} \ll 10^{-2}$ for Pe $\gg 1$.

Brownian motion dominates, simulated velocities deviate from the Henry equation values by $\leq 5.6\%$ and exhibit significant error ($\gtrsim 1\%$). However, this is attributable to statistical sampling and not a limitation of the model. In the high Péclet regime (Pe > 1) where the electrophoretic advection dominates, simulated velocities reproduce theory to within 0.71%. The results are not limited to colloidal suspensions with the exact set of properties we simulate. Rather, the model adequately describes *any* electrophoretic system in which surface conductance and double-layer distortion can be considered negligible. Furthermore, since the model performs increasingly well at large Péclet, we expect model accuracy to improve for colloidal suspensions beyond the comprehensive Péclet regime (Pe $\lesssim 10^8$) simulated.

We validate the model in the dilute regime for Pe $\gtrsim 10^{-3}$ where simulations are computationally efficient and it is reasonable to compare against the Stokes-Einstein and Henry equa-

tions. The model has not been validated in the exceedingly small Péclet regime $\mathrm{Pe} < 10^{-3}$, which, for example, is encountered in electrophoresis of aerosols. Extensions of the current model are straightforward and can be used to study polydisperse suspensions with mixtures of different colloid materials, sizes, and/or aspherical shapes. In addition, the model also can be extended to study EPD by replacing one of the periodic faces with a wall. Such particle-based mesocale EPD models could then be used to simulate an entire EPD experiment in order to elucidate optimal particle-packing strategies. However, the various treatments of the interface, e.g., a flat surface, a lattice of particles, an amorphous monolayer, surface charge heterogeneities, etc., can influence deposit microstructure in dramatically different ways. Further testing is necessary to ensure whether mesoscale particle-based models can suitably capture electrophoretic phenomena within the range of Péclet numbers pertinent to EPD additive manufacturing.

Mesoscale EPD models must mitigate the computational difficulty inherent to disparate time and length scales of bulk and deposition regimes. In comparison to the time steps we use in our current simulations, a more refined time step is required to resolve colloid-colloid and colloid-interface interactions within highly-packed deposits. Based on this work, it may be possible to model regions exclusive to the deposition while accounting for bulk electrophoretic motion by initializing the velocity of colloids with the Henry equation. Unlike bulk electrophoresis where the electric field is uniform, EPD models must treat spatial and/or temporal gradients in the applied field that may be introduced to control deposit morphology and/or arise naturally as EPD progresses. Ultimately, the interplay of all of these effects must be modeled correctly in order to reproduce the packing morphology, domain sizes, deposition times, etc., from a variety of experimental EPD systems. A mesoscale EPD model that describes extensive empirical data sets will help optimization and scale up of EPD additive manufacturing.

Acknowledgement

This work was performed under the auspices of the U.S. Department of Energy by Lawrence Livermore National Laboratory under Contract DE-AC52-07NA27344. LLNL-JRNL-669534

References

(1) Sarkar, P.; Nicholson, P. S. Electrophoretic Deposition (EPD): Mechanisms, Kinetics, and Application to Ceramics. *J. Am. Ceram. Soc.* **1996**, *79*, 1987–2002.

(2) Boccaccini, A. R.; Cho, J.; Roether, J. A.; Thomas, B. J.; Minay, E. J.; Shaffer, M. S. Electrophoretic Deposition of Carbon Nanotubes. *Carbon* **2006**, *44*, 3149–3160.

(3) Giersig, M.; Mulvaney, P. Preparation of Ordered Colloid Monolayers by Electrophoretic Deposition. *Langmuir* **1993**, *9*, 3408–3413.

(4) Qian, F.; Pascall, A. J.; Bora, M.; Han, T. Y.-J.; Guo, S.; Ly, S. S.; Worsley, M. A.; Kuntz, J. D.; Olson, T. Y. On-Demand and Location Selective Particle Assembly via Electrophoretic Deposition for Fabricating Structures with Particle-to-Particle Precision. *Langmuir* **2015**, *31*, 3563–3568.

(5) Sasaki, K. Y.; Talbot, J. B. Deposition of Powder Phosphors for Information Displays. *Adv. Mater.* **1999**, *11*, 91–105.

(6) Boccaccini, A.; Keim, S.; Ma, R.; Li, Y.; Zhitomirsky, I. Electrophoretic Deposition of Biomaterials. *J. R. Soc. Interface* **2010**, *7*, S581–S613.

(7) Reuss, F. F. Sur un Nouvel Effet de l'Électricité Galvanique. *Mem. Soc. Imp. Natur. Moscou* **1809**, *2*, 327–337.

(8) Gonzalo-Juan, I.; Krejci, A. J.; Dickerson, J. H. Toward Dynamic Control over TiO_2 Nanocrystal Monolayer-by-Monolayer Film Formation by Electrophoretic Deposition in Nonpolar Solvents. *Langmuir* **2012**, *28*, 5295–5301.

(9) D'Adamo, G.; Marenduzzo, D.; Micheletti, C.; Orlandini, E. Electric Field Controlled Columnar and Planar Patterning of Cholesteric Colloids. *Phys. Rev. Lett.* **2015**, *114*, 177801.

(10) Große-Brauckmann, J.; Lair, V.; Argirusis, C. Application of Ionic Liquids in the Electrophoretic Deposition of Oxide Layers. *Key Eng. Mat.* **2009**, *412*, 27–32.

(11) Buie, C. Electrophoretic Deposition at the Interface of Immiscible Liquids. Presented at 5th International Conference on Electrophoretic Deposition: Fundamentals and Applications, Hernstein, Austria, October 5-10, 2014.

(12) *Electrophoretic Deposition of Nanomaterials*; Dickerson, J. H., Boccaccini, A. R., Eds.; Springer: New York, 2012; Vol. 50.

(13) Pascall, A. J.; Qian, F.; Wang, G.; Worsley, M. A.; Li, Y.; Kuntz, J. D. Light-Directed Electrophoretic Deposition: A New Additive Manufacturing Technique for Arbitrarily Patterned 3D Composites. *Adv. Mater.* **2014**, *26*, 2252–2256.

(14) Nold, A.; Zeiner, J.; Assion, T.; Clasen, R. Electrophoretic Deposition as Rapid Prototyping Method. *J. Eur. Ceram. Soc.* **2010**, *30*, 1163–1170.

(15) Nold, A.; Assion, T.; Zeiner, J.; Clasen, R. Local Electrophoretic Deposition with Coaxial Electrodes. *Key Eng. Mat.* **2009**, *412*, 307–312.

(16) Qian, F.; Pascall, A. J.; Bora, M.; Han, T. Y.-J.; Guo, S.; Ly, S. S.; Worsley, M. A.; Kuntz, J. D.; Olson, T. Y. On-Demand and Location Selective Particle Assembly via Electrophoretic Deposition for Fabricating Structures with Particle-to-Particle Precision. *Langmuir* **2015**, *31*, 3563–3568.

(17) Bersa, L.; Liu, M. A Review on Fundamentals and Applications of Electrophoretic Deposition (EPD). *Prog. Mater. Sci.* **2007**, *52*, 1 – 61.

(18) Park, J. S.; Saintillan, D. Direct Numerical Simulations of Electrophoretic Deposition of Charged Colloidal Suspensions. *Key Eng. Mat.* **2012**, *507*, 47–51.

(19) Ferrari, B.; Moreno, R. EPD Kinetics: A Review. *J. Eur. Ceram. Soc.* **2010**, *30*, 1069 – 1078.

(20) Hamaker, H. Formation of a Deposit by Electrophoresis. *Trans. Faraday Soc.* **1940**, *35*, 279–287.

(21) Ferrari, B.; Moreno, R.; Cuesta, J. A. A Resistivity Model for Electrophoretic Deposition. *Key Eng. Mat.* **2006**, *314*, 175–180.

(22) Gonzalez-Cuenca, M.; Biesheuvel, P. M.; Verweij, H. Modeling Constant Voltage Electrophoretic Deposition from a Stirred Suspension. *AIChE J.* **2000**, *46*, 626–631.

(23) Pascall, A. J.; Sullivan, K. T.; Kuntz, J. D. Morphology of Electrophoretically Deposited Films on Electrode Strips. *J. Phys. Chem. B* **2013**, *117*, 1702–1707.

(24) Cordelair, J.; Greil, P. Discrete Element Modeling of Solid Formation During Electrophoretic Deposition. *J. Mater. Sci.* **2004**, *39*, 1017–1021.

(25) Einstein, A. Über die von der Molekularkinetischen Theorie der Wärme Geforderte Bewegung von in Ruhenden Flüssigkeiten Suspendierten Teilchen. *Annalen der Physik* **1905**, *322*, 549–560.

(26) Henry, D. C. The Cataphoresis of Suspended Particles Part I - The Equation of Cataphoresis. *Proc. R. Soc. A* **1931**, *133*, 106–129.

(27) Morrison, F. Electrophoresis of a Particle of Arbitrary Shape. *J. Colloid Interface Sci.* **1970**, *34*, 210–214.

(28) Hunter, R. J. *Zeta Potential in Colloid Science: Principles and Applications*; Academic Press, 2013.

(29) Groot, R. D.; Warren, P. B. Dissipative Particle Dynamics: Bridging the Gap between Atomistic and Mesoscopic Simulation. *J. Chem. Phys.* **1997**, *107*, 4423.

(30) Zhou, J.; Schmid, F. In *High Performance Computing in Science and Engineering '13*; Nagel, W. E., Kröner, D. H., Resch, M. M., Eds.; Springer, 2013; pp 5–18.

(31) Laganapan, A. M. K.; Videcoq, A.; Bienia, M.; Ala-Nissila, T.; Bochicchio, D.; Ferrando, R. Computation of Shear Viscosity of Colloidal Suspensions by SRD-MD. *J. Chem. Phys.* **2015**, *142*, 144101.

(32) Schunk, P. R.; Pierce, F.; Lechman, J. B.; Grillet, A. M.; in't Veld, P. J.; Weiss, H.; Stoltz, C.; Heine, D. R. Performance of Mesoscale Modeling Methods for Predicting Rheological Properties of Charged Polystyrene/Water Suspensions. *J. Rheol.* **2012**, *56*, 353.

(33) Bolintineanu, D. S.; Grest, G. S.; Lechman, J. B. Particle Dynamics Modeling Methods for Colloid Suspensions. *CPM* **2014**, *1*, 321–356.

(34) Plimpton, S. Fast Parallel Algorithms for Short-Range Molecular-Dynamics. *J. Comput. Phys.* **1995**, *117*, 1–19.

(35) Ball, R. C.; Melrose, J. R. A Simulation Technique for Many Spheres in Quasi-static Motion under Frame-invariant Pair Drag and Brownian Forces. *Physica A* **1997**, *247*, 444–472.

(36) Kumar, A.; Higdon, J. J. Origins of the Anomalous Stress Behavior in Charged Colloidal Suspensions under Shear. *Phys. Rev. E* **2010**, *82*, 051401.

(37) Derjaguin, B.; Landau, L. The Theory of Stability of Highly Charged Lyophobic Sols and Coalescence of Highly Charged Particles in Electrolyte Solutions. *Acta Physicochim. URSS* **1941**, *14*, 633–52.

(38) Verwey, E.; Overbeek, G. Theory of the Stability of Lyophobic Colloids. *Elsevier: Amsterdam* **1948**, *1*, 205.

(39) Everaers, R.; Ejtehadi, M. R. Interaction Potentials for Soft and Hard Ellipsoids. *Phys. Rev. E* **2003**, *67*, 041710.

(40) Safran, S. *Statistical Thermodynamics of Surfaces, Interfaces, and Membranes*; Addison-Wesley Pub., 1994.

(41) Israelachvili, J. N. *Intermolecular and Surface Forces: Revised Third Edition*; Academic Press, 2011.

(42) Probstein, R. F. *Physicochemical Hydrodynamics: An Introduction*; John Wiley & Sons, 2005.

(43) Delgado, Á. V.; González-Caballero, F.; Hunter, R.; Koopal, L.; Lyklema, J. Measurement and Interpretation of Electrokinetic Phenomena. *J. Colloid Interface Sci.* **2007**, *309*, 194–224.

(44) Schnitzer, O.; Yariv, E. Macroscale Description of Electrokinetic Flows at Large Zeta Potentials: Nonlinear Surface Conduction. *Phys. Rev. E* **2012**, *86*, 021503.

(45) Bazant, M. Z. *Induced-Charge Electrokinetic Phenomena*; Ramos, A., Eds.; Springer: Vienna, 2011; Vol. 530.

(46) Khair, A. S.; Squires, T. M. Ion Steric Effects on Electrophoresis of a Colloidal Particle. *J. Fluid Mech.* **2009**, *640*, 343–356.

(47) Reed, L.; Morrison, F. Hydrodynamic Interactions in Electrophoresis. *J. Colloid Interface Sci.* **1976**, *54*, 117–133.